CHEMISTRY
A EUROPEAN JOURNAL

DOI: 10.1002/chem.200800006

Novel Ascorbic Acid Based Ionic Liquids for the In Situ Synthesis of Quasi-Spherical and Anisotropic Gold Nanostructures in Aqueous Medium

Enakshi Dinda, Satyabrata Si, Atanu Kotal, and Tarun K. Mandal*[a]

Abstract: A series of newly designed ascorbic acid based room temperature ionic liquids were successfully used to prepare quasi-spherical and anisotropic gold nanostructures in an aqueous medium at ambient temperature. The synthesis of these room temperature ionic liquids involves, first, the preparation of a 1-alkyl (such as methyl, ethyl, butyl, hexyl, octyl, and decyl) derivative of 3-methylimidazolium hydroxide followed by the neutralization of the derivatised product with ascorbic acid. These ionic liquids show significantly better thermal stability and their glass transition temperature (T_g) decreases with increasing alkyl chain length. The ascorbate counter anion of these ionic liquids acts as a reducing agent for $HAuCl_4$ to produce metallic gold and the alkylated imidazolium counter cation acts as a capping/shape-directing agent. It has been found that the nature of the ionic liquids and the mole ratio of ionic liquid to $HAuCl_4$ has a significant effect on the morphology of the formed gold nanostructures. If an equimolar mixture of ionic liquid and $HAuCl_4$ is used, predominantly anisotropic gold nanostructures are formed and by varying the alkyl chain length attached to imidazolium cation of the ionic liquids, various particle morphologies can formed, such as quasispherical, raspberry-like, flakes or dendritic. A probable formation mechanism for such anisotropic gold nanostructures has been proposed, which is based on the results of some control experiments.

Keywords: anisotropic · ascorbic acid · gold nanostructures · ionic liquids · redox chemistry

Introduction

In the last few years, metal nanoparticles (MNPs) have been the subject of extensive research, and more particularly in the case of silver or gold nanoparticles, owing to their unique physicochemical and optoelectronic properties, which find application in the fabrication of optical devices,[1] catalysis,[2,3] surface-enhanced Raman scattering (SERS),[4] bio-labeling,[5,6] and bio-imaging.[7] Anisotropic metal nanostructures, especially, have attracted considerable interest because of their interesting size- and shape-dependent properties that make them desirable for emerging applications in fields such as optics[1] and catalysis.[2] Consequently, several different techniques including ours have been developed for preparing such anisotropic metal nanostructures with various sizes and shapes.[3,8–16] Although great strides have been made in this area, chemists and materials scientists are still searching for newer and easier methodologies for the synthesis of such anisotropic noble-metal nanostructures.

Room temperature ionic liquids (RTILs) are of current research interest because of their novel properties like negligibly small vapor pressure, high thermal stability, high chemical and electrochemical stability, and, especially at elevated temperatures, the conductivity of ionic liquids can be quite high. Although some ILs have been reported to show high stability only in a vacuum and under argon flow.[17] RTILs are generally considered as green solvents and are applied in many chemical reactions including catalysis, as well as in chemical industry as reaction solvents,[18,19] extraction solvents,[20,21] electrolytic materials,[22] etc. It is known that the physicochemical properties of ionic liquids (ILs) can be tuned by varying the chemical nature of their counter ions. Thus, up till now, to prepare ILs with new properties, many biologically relevant molecules such as amino acids,[23,24] sugar, and sugar derivatives,[25,26] lactic acids,[27,28] have been incorporated in the form of anions into the ILs.

Recently, attempts have been made to fuse two broad areas of research; the nanoparticles and the ionic liquids for the preparation of hybrid nanomaterials with novel proper-

[a] E. Dinda, Dr. S. Si, Dr. A. Kotal, Dr. T. K. Mandal
Polymer Science Unit & Centre for Advanced Materials
Indian Association for the Cultivation of Science
Jadavpur, Kolkata 700 032 (India)
Fax: (+91) 33-2473-2805
E-mail: psutkm@mahendra.iacs.res.in

Supporting information for this article is available on the WWW under http://www.chemeurj.org/ or from the author.

ties.[29–41] In a recent review, Endres et al. summarized the importance of ILs for making MNPs in this medium.[42] Owing to the nature of the ILs, the solvation of metal salts and the subsequent stabilization of the formed MNPs in the ILs are considered to be superior compared to those of conventional organic compounds.[32] Most of the ionic liquid based-MNPs syntheses involve the use of a metal ion precursor in an aqueous solution of ionic liquids followed by reduction with a conventional reducing agent.[31,33,36–41] Regardless of the importance of these MNPs, very few reports are available on their chemical synthesis, or their electro deposition using ionic liquids as reaction medium.[29,30,43–49] However, the in situ formation of MNPs in aqueous solution by using ILs that have a redox-active counter anion are very limited. For example, Kim et al have reported the preparation of gold nanoparticles (GNPs) by using alcohol-based ILs in water.[33] Thus, a room temperature synthesis of noble MNPs (e.g. gold, silver, and platinum) by using redox active ILs still waits to dominate/occupy an active area in nanoparticles research.

Recently, our research group has been actively involved in the synthesis of MNPs using tyrosine/tryptophan-based peptides by in situ reduction approach in aqueous medium.[50–53] This encouraged us to explore the in situ reduction technique further to synthesize MNPs using newly designed redox-active ILs as reducing/stabilizing agents. It is known that ascorbic acid generally exhibits keto-enol tautomerisim, the enol form of which is susceptible to ionization in aqueous solution and has been used as a versatile reducing agent for variety of metal ion precursors to prepare MNPs.[54–58] Thus, the choice of an appropriate cationic species to conjugate with the ionic form of ascorbic acid is crucial for the synthesis of RTIL, which in turn can be utilized to prepare MNPs by in situ reduction in the absence of any externally added reducing agents.

In the present work, we report the synthesis of a series of novel ascorbic acid based ionic liquids (ILs). These newly designed ILs are then utilized to prepare anisotropic gold nanostructures of various morphologies as well as quasi-spherical GNPs in aqueous medium. The effect of mole ratio of IL to gold salt on the morphology of the formed gold nanostructures has also been investigated.

Results and Discussion

The ascorbic acid based room temperature ionic liquids (RTILs) were prepared by the modification of the Ohno method.[24] Table 1 depicts the chemical name of all the ILs that have been synthesized and used for the generation of GNPs. The synthesis of these RTILs involves, initially, the preparation alkyl derivative of imidazolium hydroxide followed by neutralization with the ascorbic acid (see Scheme 1). The synthesized ILs were characterized by ^{1}HNMR spectroscopy, ESI mass spectrometry, and also by elemental analysis. The ^{1}HNMR spectrum of neat ascorbic acid in [D_6]DMSO shows a doublet peak at around $\delta =$ 4.62 ppm, which corresponds to the five member ring proton of ascorbic acid. However, in case of sodium ascorbate in D_2O, this peak shows an up-field shift of 0.24 ppm ($\delta = 4.62$ to 4.38 ppm). This shift is a result of the presence of the enol form of ascorbic acid in sodium ascorbate solution. The ^{1}HNMR of IL, [C_2mim][A] (for definitions please see Table 1) in D_2O also shows a similar doublet peak at around $\delta = 4.40$ ppm. This result also indicates and confirms the presence of enol form of ascorbic acid in this IL. However, the ^{1}HNMR spectra of the ILs performed in DMSO did not show such types of peaks, rather a broad peak appeared in the region $\delta = 3$–4 ppm, as a result of the DMSO. This broad peak probably masks the peak produced by the enol form of ascorbic acid. The ESI mass spectral data of the as-prepared ILs show the presence of a strong signal (as indicated in the Experimental Section), which belongs to the cationic part of the corresponding IL and no other peaks were traced in the ESI mass spectra and further confirms the purity of the ionic liquids (see the Supporting Information for spectra). All the synthesized ILs are initially dark-brown colored, highly-viscous materials at room temperature and hygroscopic in nature. The presence of some impurities might be responsible for such color. It has been reported that the presence of ppm levels of impurity affects the properties of ILs.[59] In our case, after purification with active charcoal powder, the ILs became colorless. These ILs are soluble in most polar solvents, such as water, methanol, DMSO, DMF etc.

Table 1. Chemical names of all the synthesized ILs and their glass transition temperatures (T_g).

Ionic Liquid	Name	T_g [°C]
1-methylimidazolium ascorbate	[C_0mim][A]	6.89
1-ethyl-3-methylimidazolium ascorbate	[C_2mim][A]	−28.47
1-butyl-3-methylimidazoliumascorbate	[C_4mim][A]	−21.48
1-hexyl-3-methylimidazolium ascorbate	[C_6mim][A]	−32.33
1-octyl-3-methylimidazolium ascorbate	[C_8mim][A]	−34.94
1-decyl-3-methylimidazoliumascorbate	[C_{10}mim][A]	−42.34

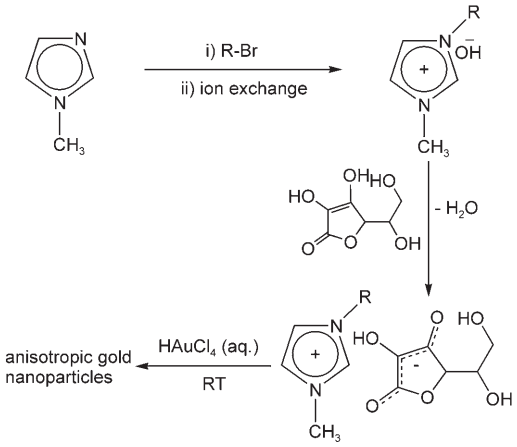

Scheme 1. R = H, C_2H_5, C_4H_9, C_6H_{13}, C_8H_{17}, and $C_{10}H_{21}$.

Figure 1 shows the thermogravimetric analysis (TGA) curve of the purified ILs, ([C_2mim][A], [C_6mim][A], and [C_{10}mim][A]), which exhibits the decomposition tempera-

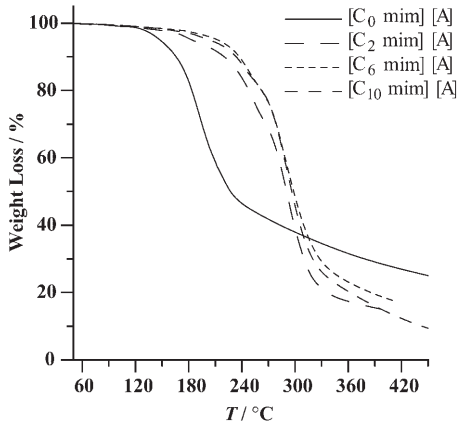

Figure 1. TGA thermograms of different ascorbic acid based ionic liquids.

tures at around 240 °C and is close to that observed for the reported amino acid-based ILs.[23,24] The introduction of an alkyl chain in the imidazolium cation results in a drastic increase in the decomposition temperature (≈240 °C) of the ILs compared to that of an IL without any alkyl groups, [C_0mim][A] (≈180 °C). However, an increase in the substituted alkyl chain length has almost no effect on the decomposition temperature of all of the synthesized ILs and they all decompose within nearly the same temperature range (see the TGA thermograms given in Figure 1).

Furthermore, thermal-transition behaviors of these ascorbic acid based ILs were examined by differential-scanning calorimetry (DSC). The DSC thermograms are shown in Figure 2 and show that each of these ILs exhibit a sharp glass transition temperature (T_g). Table 1 depicts the T_g (onset) of all the ILs. These data clearly reveal that an increase in the length of the substituted alkyl chain of the imidazolium cation, decreases the T_g value of the IL with a slight deviation in case of [C_2mim][A]. It has been reported that the imidazolium-based ILs with shorter alkyl chains ($n=2$–11) are liquid at room temperature and transform to glassy form on cooling to −80 °C, whereas those with comparatively longer alkyl chains ($n=12$–18) are low melting solids and showed a mesophase upon heating.[60] Therefore, we can assume that the length of the alkyl chain attached to imidazolium ion is responsible for such variation of T_g in these ILs. Furthermore, we did not observe any crystalline melting temperatures (T_m) for any of these ILs. According to the literature, the T_m of an IL strongly depends on the choice of anions.[61] In this case, the large ascorbate ion present in between two layers of imidazolium ions disturbs the local molecular ordering of the ILs and this may be the reason for the absence of any T_m values in our synthesized ILs.

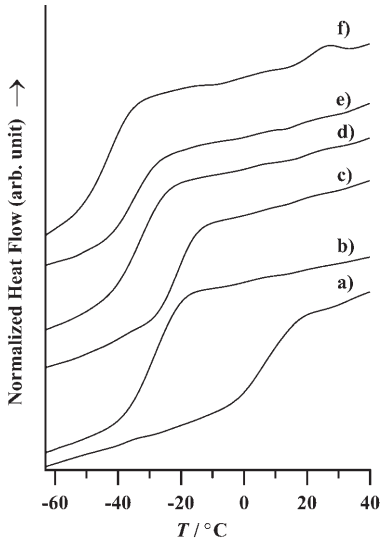

Figure 2. DSC thermograms of different ascorbic acid based ionic liquids: a) [C_0mim][A], b) [C_2mim][A], c) [C_4mim][A], d) [C_6mim][A], e) [C_8mim][A], and f) [C_{10}mim][A].

The FTIR spectrum of a representative IL, [C_6mim][A] shown in Figure 3 indicates that the stretching frequency of >C=O and >C=C< groups of neat ascorbic acid shifted

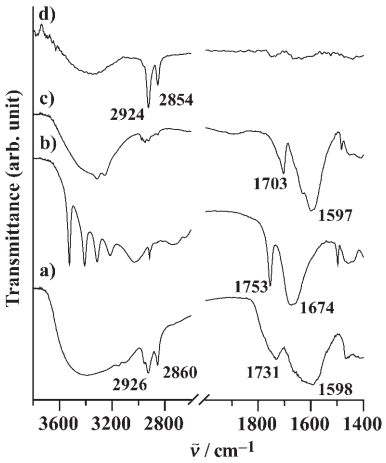

Figure 3. FTIR spectra of a) [C_6mim][A], b) neat ascorbic acid, c) neat sodium ascorbate, and d) gold nanostructures coated with the [C_6mim] cation.

from $\tilde{\nu}=1753$ to 1731 cm^{-1} and $\tilde{\nu}=1674$ to 1598 cm^{-1} respectively after IL formation (compare Figure 3a and 3b). A similar shifting was also observed for sodium ascorbate (compare Figure 3b and 3c). These results confirm that ILs are formed by the combination of alkyl imidazolium cation and ascorbate anion, where the latter exists as a keto-enol tautomeric form. The FTIR spectrum of the hexyl substituted imidazolium cation containing gold nanostructures is shown in Figure 3d, the detailed analysis of which will be discussed latter in this section.

The reducing property of ascorbic acid is well understood and has been used for generations of MNPs, mainly in an alkaline medium.[54–57] However, the morphologies of the formed MNPs are mostly spherical in nature. As mentioned above, in these newly designed ILs the ascorbic acid exists as a negatively charged ascorbate ion and is, therefore, expected to be a better reducing agent than the neat ascorbic acid. Furthermore, the presence of alkyl substituted imidazolium cation may influence the formation mechanism, which might result in the formation of anisotropic gold nanostructures of various morphologies. Also in this method, it is not necessary to make the medium alkaline, as the ascorbic acid remains in the ionized form. Thus, we have tried to utilize these newly designed ascorbic acid based ILs to synthesize gold nanostructures with the expectation that these ILs may give rise to the formation of different shaped GNPs.

The synthesis of gold nanostructures involves the simple aqueous-phase mixing of ascorbic acid based ILs and $HAuCl_4$ at room temperature (see Table 2 for more details).

Table 2. Detailed reaction recipes for the synthesis of gold nanostructures at different mole ratios of IL to $HAuCl_4$.

Set	ILs [mM]	$HAuCl_4$ [mM]	$R=$[ILs]/[$HAuCl_4$]
1	0.5[a]	0.5	1.0
2	0.125[b]	0.5	0.25
3	2.0[c]	0.5	4.0

[a] ILs used: [C_0mim][A], [C_2mim][A], [C_4mim][A], [C_6mim][A], [C_8mim][A], and [C_{10}mim][A]; [b] ILs used: [C_2mim][A], [C_4mim][A], [C_6mim][A], [C_8mim][A], and [C_{10}mim][A]; [c] ILs used: [C_2mim][A], [C_4mim][A], [C_6mim][A], [C_8mim][A], and [C_{10}mim][A].

The progress of the reactions between aqueous solution of $HAuCl_4$ and ILs was monitored visually and by means of UV/Vis spectroscopy. A faint color developed immediately after the addition of IL to the aqueous $HAuCl_4$ solution and became more intense over time. A stable color was observed within 3 min of reaction, this is an indication of the formation of nanosized metallic gold. This result also indicates that the reaction is very fast. This concurs with the kinetic studies of formation of these gold nanostructures discussed later in this section. The color of the suspension was varied and dependent on type of ILs used i.e., pink, purple, and gray respectively for [C_2mim][A], [C_6mim][A], and [C_{10}mim][A] and pink and gray respectively for [C_4mim][A] and [C_8mim][A]. However, the time required to develop a stable color of the gold nanostructure suspension depends on the R (mole ratio of ILs to $HAuCl_4$) values, that is, at increasing values of R, the reaction develops more quickly.

The stability of the colloidal gold nanostructures′ suspension depends upon the length of alkyl chain attached to the imidazolium ion of ILs. For example, a suspension of gold nanostructures, prepared with [C_2mim][A] using $R=1$, is stable for 5 days without any precipitation, whereas those prepared with [C_{10}mim][A] are less stable and precipitation can occur within 12 hours. These observations indicate that as the alkyl chain length of the imidazolium ion of ILs increase, the stability of the suspension of colloidal gold nanostructures decreases.

A set of UV/Vis spectra of the as-prepared suspension of colloidal gold nanostructures prepared at $R=$([IL]/[$HAuCl_4$])$=1$ (see reaction Set 1 in Table 2) recorded after 15 min of reaction can be seen in Figure 4. The spectra of all the samples in aqueous suspension show the presence of a

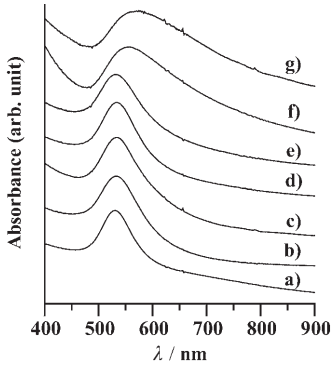

Figure 4. UV/Vis absorption spectra of different as-prepared suspensions of gold nanostructures prepared with a) sodium ascorbate, b) [C_0mim][A], c) [C_2mim][A], d) [C_4mim][A], e) [C_6mim][A], f) [C_8mim][A], and g) [C_{10}mim][A] at a value of $R=1$.

broad surface plasmon resonance (SPR) absorption band in the wavelength region $\lambda=500$–600 nm indicating the formation of different-shaped gold nanostructures other than spheres. More specifically, the as-prepared samples that were synthesized with ILs exhibit a slightly broad SPR band accompanied by a long tail at $\lambda_{max}=532$, 533, 534, 534, 553, and 574 nm, for [C_0mim][A], [C_2mim][A], [C_4mim][A], [C_6mim][A], [C_8mim][A] and [C_{10}mim][A], respectively (see Figure 4). For comparison, we have also prepared gold nanoparticles (GNPs) with sodium ascorbate, the aqueous suspension of which exhibits a sharp SPR band at $\lambda=$ 530 nm without any tailing (see Figure 4a). These optical results suggest that the gold nanostructures prepared with ILs should possess different morphology than those prepared with neat sodium ascorbate. To confirm this issue, we examined the morphologies of these gold nanostructures by means of TEM and the results will be discussed in detail later in this section. The SPR band position of GNPs prepared with [C_0mim][A], [C_2mim][A], [C_4mim][A] and [C_6mim][A] (see Figures 4b–e, respectively) are essentially in the same region ($\lambda=532$–534 nm), whereas those prepared with [C_8mim][A] (Figure 4g) and [C_{10}mim][A] (Figure 4f) show a significant shift in the SPR band position to $\lambda_{max}=553$ and 574 nm, respectively.

To check the effect of variation mole ratio of ILs to $HAuCl_4$ on the nature of spectra of formed gold nanostructures, we first carried out reduction of $HAuCl_4$ with different ILs by decreasing the mole ratio to $R=$[IL]/[$HAuCl_4$]$=0.25$ (see reaction Set 2 in Table 2). The UV/Vis spectra showed a sharp SPR band at $\lambda_{max}=530$, 532 and 535 nm for GNPs

prepared in reaction with ILs, [C_2mim][A], [C_4mim][A], and [C_6mim][A] respectively (see Figures 5a–c) indicating the formation of mostly spherical particles, but the SPR bands

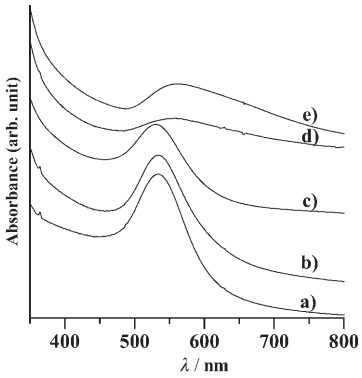

Figure 5. UV/Vis absorption spectra of the as-prepared suspensions of gold nanostructures prepared with different ILs a) [C_2mim][A], b) [C_4mim][A], c) [C_6mim][A], d) [C_8mim][A], and e) [C_{10}mim][A] at a value of $R=0.25$.

were suddenly broadened for GNPs prepared with [C_8mim][A] and [C_{10}mim][A] (see Figure 5d and 5e, respectively).

However, upon increasing the concentration of ILs in the reaction mixture to $R=4$ (see reaction Set 3 in Table 2), a slightly different spectral pattern was observed. The UV/Vis spectra of the suspensions of gold nanostructures prepared with [C_2mim][A] and [C_4mim][A] show the presence of a sharp SPR absorption band at $\lambda=528$ and 532 nm respectively (see Figure 6a,b). Gold nanostructures prepared by using [C_6mim][A], produce a sharp SPR band at $\lambda=532$ nm

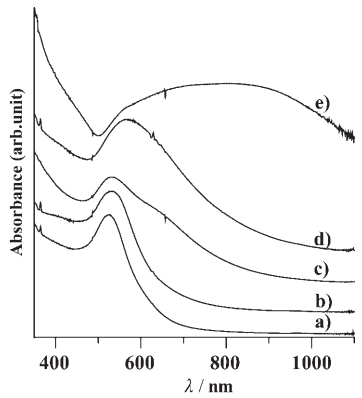

Figure 6. UV/Vis absorption spectra of the as-prepared suspensions of gold nanostructures prepared with a) [C_2mim][A], b) [C_4mim][A], c) [C_6mim][A], d) [C_8mim][A], and e) [C_{10}mim][A] at a value of $R=4$.

that is accompanied by a second absorption band in the higher wavelength region ($\lambda\approx700$ nm) (see Figure 6c). Whereas, gold nanostructures prepared with ILs that have a long chain alkyl group ([C_8mim][A] and [C_{10}mim][A]) produced a large broadening in the SPR band (see Figure 6d,e). These shifting of SPR bands of gold nanostructures, suspension, prepared with [C_8mim][A] and [C_{10}mim][A], may be attributed to either the formation of the aggregated structure, or to the branching of gold nanostructures as mentioned elsewhere.[62]

The kinetics of gold nanostructure formation was studied via recording the time dependent UV/Vis spectra of the their colloidal suspensions during their formation. As a representative case, we have only studied the kinetics of formation of gold nanostructures that are prepared at $R=$[IL]/[$HAuCl_4$]$=1.0$ (see Table 2). For the samples prepared with the ILs [C_2mim][A] and [C_6mim][A] the variation of absorbance values at $\lambda_{max}=530$ nm were plotted against time (see Figures 7a and 7b respectively). For samples prepared with [C_{10}mim][A], the kinetics of formation was studied by measuring the change in absorbance value at $\lambda_{max}=567$ nm of the SPR band (Figure 7c). It is clear that the formation of gold nanostructures started immediately after the addition of the respective ILs (see Figures 7a–c). The insets of these figures represent an enlarged view of the early time segment and indicate a sudden jump in the absorbance value after 3 minutes of the reaction. Notably, in three cases, the absorbance values remain unchanged after 10 minutes of the reaction (see Figures 7a–c). These results indicate that the reactions between these ILs and $HAuCl_4$ are very fast and almost complete within a 10 min time span. For comparison, the kinetics of formation of GNPs prepared with neat sodium ascorbate is also presented (see Figure 7d). The inset of Figure 7d shows no such jump in the absorbance value as noticed in the earlier cases. Such a fast reaction between the

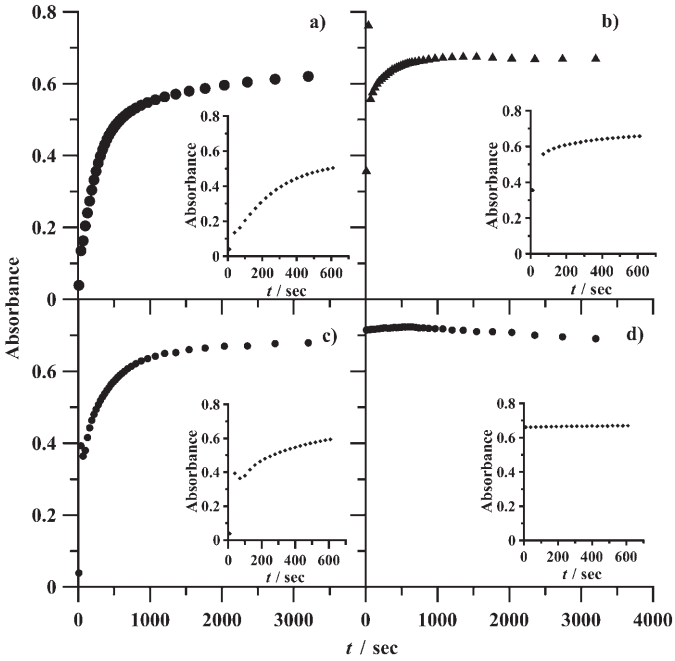

Figure 7. UV/Vis kinetics of gold nanostructure formation using different ILs: a) [C_2mim][A], b) [C_6mim][A], c) [C_{10}mim][A] and d) neat sodium ascorbate. Insets show the enlarged view for the lower-time region.

IL and $HAuCl_4$ might be responsible for the formation of different shaped-GNPs as can be seen from TEM image analysis discussed later in this section.

The representative TEM micrographs of gold nanostructures prepared with different ionic liquids following the conditions ($R = [IL]/[HAuCl_4] = 1.0$) given in reaction Set 1 (see Table 2) are shown in Figure 8. From these images, it is apparent that the particles synthesized with [C_0mim][A] are

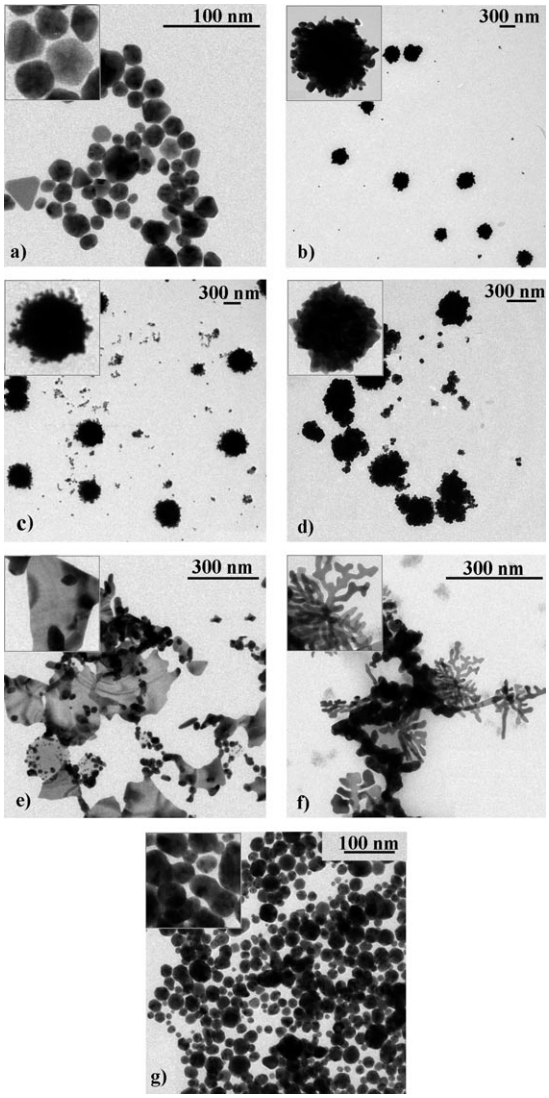

Figure 8. TEM micrographs of gold nanostructures prepared with: a) [C_0mim][A], b) [C_2mim][A], c) [C_4mim][A], d) [C_6mim][A], e) [C_8mim][A], f) [C_{10}mim][A], and g) neat sodium ascorbate at mole ratio value of $R = 1$ (see Set 1). Insets show the enlarged view of the respective particles.

mostly quasi-spherical in shape (Figure 8a), whereas those synthesized with [C_2mim][A], [C_4mim][A], and [C_6mim][A] are of almost similar morphology and resemble raspberry-like nanostructures (Figures 8b–d). For the latter three samples, it is expected that the nature of the SPR band would be the same as the morphology looks like the same. However, as shown earlier that the SPR band of GNPs prepared with [C_0mim][A] (Figure 4b) compared with the bands produced from [C_2mim][A], [C_4mim][A] and [C_6mim][A] (Figure 4c—e, respectively) are almost alike in terms of their nature and position. Furthermore, the TEM images of gold nanostructures prepared with [C_8mim][A] and [C_{10}mim][A] show flake and dendrite like morphology, respectively (Figure 8e,f). This might be the reason that the SPR bands for the suspensions of these two samples are red-shifted and broaden, compared to those of samples prepared with ILs containing an hexyl chain or shorter (see Figure 4f,g). The insets of Figures 8b–e show the enlarged view of the respective single anisotropic nanostructure, which apparently indicate that each of these structures are formed as a result of aggregation or assembly of smaller spherical particles. However, the sample prepared by using sodium ascorbate under similar reaction conditions shows only quasi-spherical particles (Figure 8g). Thus, the gold nanostructures synthesized with ionic liquids that have shorter alkyl chains form quasi-spherical morphology, whereas those with longer alkyl chains result in the formation of anisotropic nanoparticles.

If the value of R is decreased to 0.25 (see reaction Set 2 in Table 2) the TEM images of the samples prepared with [C_2mim][A], [C_4mim][A] and [C_6mim][A] (see Figures 9a–c, respectively) displayed mostly quasi-spherical nanoparticles (with some aggregation), but did not show any anisotropic

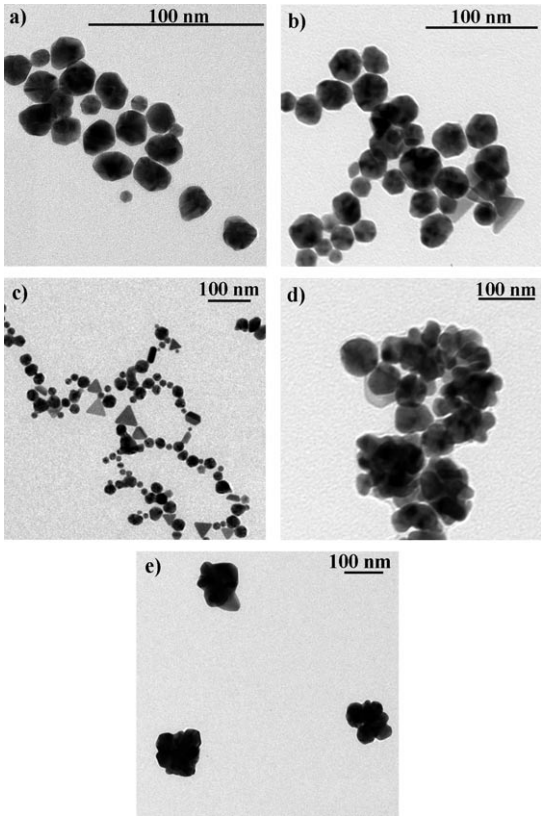

Figure 9. TEM micrographs of gold nanostructures prepared with: a) [C_2mim][A], b) [C_4mim][A], c) [C_6mim][A], d) [C_8mim][A], and e) [C_{10}mim][A] at a value of $R = 0.25$.

nanostructures. However, in the case of sample prepared with [C_8mim][A], it appears that they have a certain anisotropy in their shape (Figure 9d). This anisotropy in shape is more prominent in the case of the gold nanostructures that were prepared by using [C_{10}mim][A] (Figure 9e). It again indicates that each of the structure in Figure 9e, are formed as a result of aggregation or the assembly of smaller particles, as observed for gold nanostructures prepared at $R=1$ by using [C_2mim][A], [C_4mim][A] and [C_6mim][A] ILs.

The TEM images of all the samples prepared at $R=4.0$ (see reaction Set 3 in Table 2) is represented in Figure 10. In this case, again mostly quasi-spherical particles are formed along with some aggregation of these particles were also observed if [C_2mim][A], [C_4mim][A] and [C_6mim][A] are used (see Figures 10a–c, respectively). Whereas, for the samples

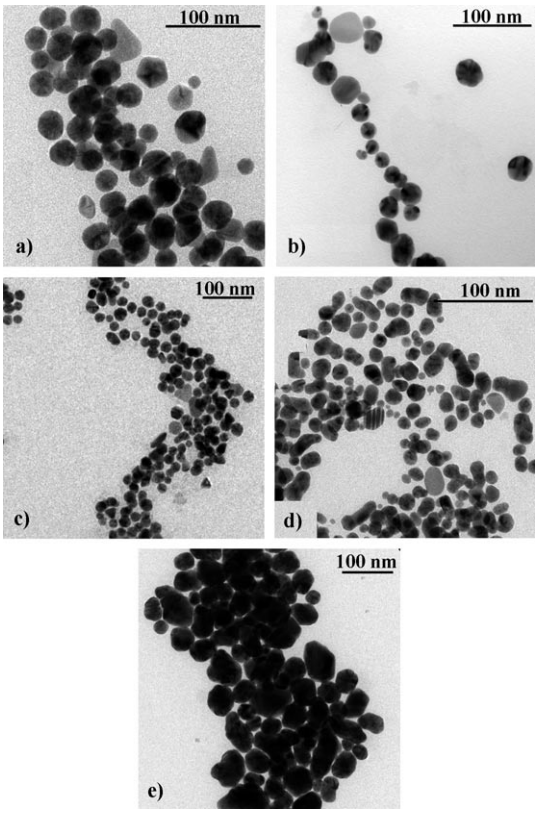

Figure 10. TEM micrographs of gold nanostructures prepared with: a) [C_2mim][A], b) [C_4mim][A], c) [C_6mim][A], d) [C_8mim][A], e) [C_{10}mim][A] at a value of $R=4$.

prepared with [C_8mim][A] and [C_{10}mim][A] a mixture of quasi-spherical and irregular shaped nanoparticles are formed. These as-formed particles are not well dispersed and they have a tendency to form agglomerates.

From the analysis of TEM and optical results, it may be concluded that the ascorbate ion of the IL reduces Au^{3+} to metallic Au and that the alkyl substituted imidazolium cation plays a crucial role in the shape evaluation. The mole ratio (R) of IL to $HAuCl_4$ also plays an important role in the ultimate shape determination.

To get better understanding of the effect of the alkyl substituted imidazolium cation on the morphology of formed gold nanostructures, we have carried out the reduction of gold salt using ILs in presence of an water-soluble polymer, poly(vinyl pyrrolidone) (PVP) that can also act as a stabilizer. Typical TEM micrographs of the samples prepared by using [C_2mim][A], [C_6mim][A] and [C_{10}mim][A] at $R=1.0$ (e.g., [IL]=[$HAuCl_4$]=0.5 mM) in presence of PVP (0.1 wt%) are shown in Figure 11. The formation of solely spherical gold nanoparticles (GNPs) when prepared using [C_2mim][A] and [C_6mim][A] ILs respectively can be seen in Figures 11a,b. This might be a result of the bulky PVP molecules absorbed onto the surface of the GNP, hindering the GNPs from the anisotropic crystal growth, by preventing coalescence between initially formed spherical particles. The

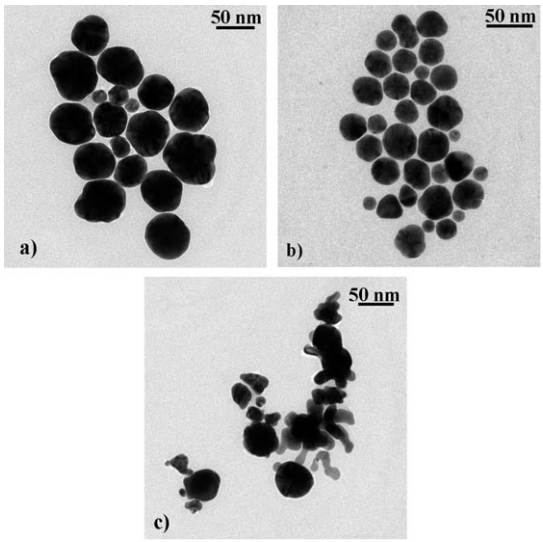

Figure 11. TEM micrographs of gold nanoparticles prepared in presence of PVP using the ILs: a) [C_2mim][A], b) [C_6mim][A], and c) [C_{10}mim][A] at a value of $R=1$.

polymer PVP in presence of [C_{10}mim][A] formed particles that have a little tendency to form dendritic structures (see Figure 9c). However, owing to the presence of bulky polymeric chains, further growth to the dendritic structure was hindered. Again, the GNPs prepared with these ILs at concentrations of PVP greater than 0.1 wt% formed particles that stuck to the reaction vessel. This might be owed to the cationic part of ILs interacting with PVP to prevent the GNPs from proper stabilization.

Wide angle X-ray characterization was carried out on these gold nanostructure samples obtained according to reaction Set 1 (see Table 2) to provide support for such anisotropic growth. The X-ray diffraction (XRD) patterns of the samples prepared by using different ILs (e.g., [C_2mim][A], [C_6mim][A], and [C_{10}mim][A]) as a reducing/structure-directing agent can be seen in Figure 12. All the samples showed an intense peak at $2\theta=38.2$, which corresponds to the (111) lattice plane of the fcc metallic gold. Whereas the

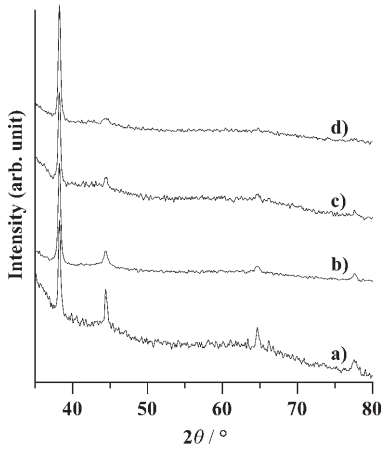

Figure 12. XRD pattern of gold nanostructures prepared by using a) sodium ascorbate, b) [C_2mim][A], c) [C_6mim][A], and d) [C_{10}mim][A] at a value of $R=1$.

peaks at $2\theta=44.4$, 64.7, 77.6, correspond to the lattice planes (200), (220), and (311) of Au, are very weak. These data reveal that with an increase in length of the substituted alkyl chain of ILs, the intensity of the peak that belongs to the (111) plane of the formed gold nanostructure increases and at the same time other peaks gradually diminish. These results indicate that the growth along (111) plane becomes more pronounced in comparison to the other planes. This type of unidirectional growth along the (111) plane might be responsible for the formation of anisotropic gold nanostructures of different morphologies. Also, the presence of long hydrophobic chain in the IL might assist the unidirectional growth of gold nanostructure that resulted in the formation of various morphologies.

In these reactions $HAuCl_4$ is reduced by the ascorbate ion of the ILs in the absence of any externally added reducing agents. During the reduction, the ascorbate ion is converted to its oxidized form, as reported earlier,[54–58] whereas the alkylated imidazolium cation has a chance to adsorb to the negatively charged surface of newly formed small gold particulates, which eventually combine to form bigger gold nanostructures. This was confirmed by FTIR characterization of the precipitated/washed gold nanostructures prepared with [C_6mim][A] and the spectra are presented in Figure 3d. The spectra did not show any bands corresponding to the $>C=O$ stretching vibration of the ascorbate ion or any characteristic band of the oxidized form of ascorbate ion (compare Figures 3c and 3d). The vibration owed to the $-CH_2-$ group of the substituted hexyl chain is very prominent indicating the attachment of the cationic part of the IL on the surface of the GNPs (Figure 3d).

On the basis of these results, we can propose a probable mechanism of growth of such anisotropic gold nanostructures. The initially formed smaller particles are hydrophobic in nature, as a result of the adsorption of alkylated imidazolium groups onto the surface. The hydrophobic nature of the smaller particles makes them poorly soluble in the aqueous dispersion, which results in the formation of anisotropic nanoparticles throughout the coalescence of these unstable particles till the system attains a minimum energy. Furthermore, the enlarged view of TEM images of all the samples except those prepared with [C_0mim][A] (see insets of Figures 8b–f) show that these anisotropic gold nanostructures consist of smaller spherical particles. The gold nanostructures prepared with [C_8mim][A] and [C_{10}mim][A] show some unique flake- and dendrite-like growth (see insets of Figure 8e and 8f).

Conclusion

In this article, our approach has been directed towards the synthesis of quasi-spherical and anisotropic gold nanostructures of various morphologies by using a series of newly designed ascorbic acid based ionic liquids (ILs) as a reducing agents as well as structure-directing agents. In this case, ascorbate ion acts as a reducing agent and the alkylated imidazolium ion acts as capping/structure-directing agent, which we confirmed by means of FTIR spectroscopy analysis. With the variation of the length of the alkyl chain attached to the imidazolium cation, the particle morphology (spherical/raspberry/flake/dendritic) of the gold nanostructures was successfully tuned. However, the mole ratio of ILs to $HAuCl_4$ has a significant effect on the morphology of formed gold nanostructures. These newly designed ILs are excellent reducing agents and can be used for the in situ generation of a wide range of metal nanostructures.

Experimental Section

General: Ascorbic acid, 1-methylimidazole, ethyl bromide, butyl bromide, hexyl bromide, octyl bromide, decyl bromide, poly(vinyl pyrrolidone) (PVP), and hydrogen tetrachloroaurate (III) trihydrate ($HAuCl_4 \cdot 3H_2O$) were purchased from Sigma–Aldrich and were used without further purification. All the aqueous solutions were prepared with triple-distilled water and distilled reagent grade solvents were used for the ionic liquid synthesis.*NMR spectroscopy*: ^{1}HNMR studies of all the ILs, neat ascorbic acid, and neat sodium ascorbate were carried out by using a Bruker DPX 300 MHz spectrometer.

Elemental analysis: Elemental analyses of the purified 1-alkyl-3-methylimidazolium bromides and their corresponding ascorbate ILs were carried out by using a Perkin–Elmer 2400 series II CHN analyzer.

ESI mass spectrometry: The ESI mass spectra of the synthesized 1-alkyl-3-methylimidazolium bromides and 1-alkyl-3-methylimidazolium ascorbates were recorded from a methanol solution in a Quadrupole time-of-flight (Qtof) Micro YA263 mass spectrometer.

Thermogravimetric analysis (TGA): TGA thermograms of all the ILs were recorded by using a TA SDT Q600 instrument at a heating rate of $20\,^\circ C\,min^{-1}$ under a N_2 atmosphere.

Differential scanning calorimetry (DSC): The glass transition temperature (T_g) of the ILs was measured using a Perkin–Elmer Diamond DSC equipped with an intercooler at a scan rate of $20\,^\circ C\,min^{-1}$. For all samples, at least one cycle of heating and cooling were performed before taking the final heating scan. Note that the ILs were dried at 70 °C in vacuum for three days before the DSC measurements.

UV/Vis absorption spectroscopy: UV/Vis absorption spectra of the suspension of the gold nanostructures prepared with different ILs were re-

corded in a Hewlett Packard 8453 diode-array UV/Vis spectrophotometer.

Transmission electron microscopy (TEM): One drop of the as-prepared suspension of the gold nanostructures prepared with different ILs was placed on a carbon-coated copper grid and allowed to air-dry at room temperature. The grid was then observed under a JEOL JEM 2010 high-resolution transmission electron microscope at an accelerating voltage of 200 kV.

X-Ray diffraction (XRD): For XRD analysis, the different as-prepared suspensions of gold nanostructures were deposited on a microscopic glass slide and the diffractograms were then recorded by using a Seifert XRD 3000P diffractrometer at an accelerating voltage of 35 kV by using a $Cu_{k\alpha}$ ($\lambda = 1.54$ Å) as the X-ray radiation source.

Fourier Transform Infrared (FTIR) Spectroscopy: FTIR spectra of neat ascorbic acid, sodium salt of ascorbic acid, ionic liquid and the centrifuged/washed/dried gold nanostructures prepared with ILs were recorded using KBr pellets in a Shimadzu FTIR-8400S spectrometer. The pellets were prepared by mixing the corresponding dried sample with KBr in a 1:100 (w/w) ratio.

Synthesis of ionic liquids:

Synthesis of 1-alkyl-3-methylimidazolium bromide: In a typical synthesis, a mixture of 1-methylimmidazole (10 mM) and any alkyl bromide (10 mM) (such as ethyl bromide, butyl bromide, hexyl bromide, octyl bromide, and decyl bromide) was refluxed at 70°C for 36 h with continuous magnetic stirring. The resultant yellowish viscous compound was then washed thoroughly with distilled diethyl ether four times for complete removal of unreacted components. Finally, a pale- white waxy solid mass was obtained. All the purified 1-alkyl-3-methylimidazolium bromides were then dried in a vacuum and characterized by 300 MHz ^{1}H NMR spectroscopy ($CDCl_3$) and ESI mass spectroscopy.

1-Ethyl-3-methylimidazolium bromide: ^{1}H NMR (300 MHz, $CDCl_3$, TMS): $\delta = 10.41$ (s,Immidazole ring H), 7.43–7.42 (m, Immidazole ring H), 4.46–4.38 (q, $J = 7.4$ Hz, -NCH_2), 4.12 (s, -NCH_3), 1.63–1.59 ppm (t, $J = 7.3$ Hz, -CH_3); MS (EI, 35 eV): m/z: 111 (M^+ 100%).

1-Butyl-3-methylimidazolium bromide: ^{1}H NMR (300 MHz, $CDCl_3$, TMS): $\delta = 10.25$ (s, Immidazole ring H), 7.61 (s, Immidazole ring H), 7.49 (s, Immidazole ring H), 4.37–4.32 (t, $J = 7.5$ Hz, -NCH_2), 4.15 (s, -NCH_3), 1.96–1.86 (m, -CH_2), 1.43–1.36 (m, -CH_2), 0.99–0.94 ppm (t, $J = 7.3$ Hz, -CH_3); MS (EI, 35 eV): m/z: 139 (M^+ 100%).

1-Hexyl-3-methylimidazolium bromide: ^{1}H NMR (300 MHz, $CDCl_3$, TMS): $\delta = 10.20$ (s, Immidazole ring H), 7.53 (s, Immidazole ring H), 7.39 (s, Immidazole ring H), 4.35–4.30 (t, $J = 7.4$ Hz, -NCH_2), 4.13 (s, -NCH_3), 1.94–1.89 (m, -CH_2), 1.32 (bs, 3-CH_2), 0.90–0.86 ppm (t, $J = 7.3$ Hz, -CH_3); MS (EI, 35 eV): m/z: 167 (M^+ 100%).

1-Octyl-3-methylimidazolium bromide: ^{1}H NMR (300 MHz, $CDCl_3$, TMS): $\delta = 10.43$ (s, Immidazole ring H), 7.58–7.55 (d, $J = 9.0$ Hz, Immidazole ring H), 7.42–7.39 (d, $J = 9.0$, Immidazole ring H), 4.35–4.30 (t, $J = 7.4$ Hz, -NCH_2), 4.14 (s, -NCH_3), 1.94–1.89 (m, -CH_2), 1.32–1.25 (bs, 5-CH_2), 0.89–0.85 ppm (t, $J = 7.0$ Hz, 3H); MS (EI, 35 eV): m/z: 195 (M^+ 100%).

1-Decyle-3-methylimidazolium bromide: ^{1}H NMR (300 MHz, $CDCl_3$, TMS): $\delta = 10.61$ (s, 1H), 7.31 (s, 1H), 7.24 (s, 1H), 4.34–4.29 (t, $J = 7.4$ Hz, 2H), 4.13 (s, 3H), 1.92 (m, 2H), 1.25 (bs, 14H), 0.90–0.85 ppm (t, $J = 6.3$ Hz, 3H); MS (EI, 35 eV): m/z: 223 (M^+ 100%).

Synthesis of 1-alkyl-3-methylimidazolium hydroxide: 1-alkyl-3-methylimidazolium hydroxides were prepared by passing the corresponding aqueous 1-alkyl-3-methylimidazolium bromides solution (5 mM) through anion exchange resin (Amberlite IRA-400Cl, Aldrich). For this, a glass column was first packed with the resin followed by washing with plenty of water. The column was charged with an aqueous NaOH solution (2 M) to modify the resin beads with hydroxide ions. The column was then washed thoroughly with water to remove any traces of unexchanged hydroxide ion (tested with Litmus paper). Finally, an aqueous solution of 1-alkyl-3-methylimidazolium bromide was passed through the column to exchange the bromide ions with hydroxide ions. The exchange reaction was confirmed by means of thin layer chromatography (TLC).

Synthesis of 1-alkyl-3-methylimidazolium ascorbate ionic liquids: In a typical synthesis of 1-alkyl-3-methylimidazolium ascorbate, solid ascorbic acid (5 mM) was added to an as prepared aqueous solution of 1-alkyl-3-methylimidazolium hydroxide (5 mM) and the reaction mixture was stirred magnetically for 12 h at room temperature. The resultant 1-alkyl-3-methylimidazolium ascorbates were isolated through freeze-drying process. Finally, all the ascorbic acid based ILs (as depicted in Table 1) were dissolved in a mixed solvent of methanol/acetonitrile (1:9) and filtered to remove the residual solid impurities. The resultant ILs were dark-brown and viscous.

Purification of ascorbic acid based ILs: An IL (1 g) was dissolved in distilled methanol (5 mL) followed by the addition of active charcoal powder (10 g). The mixture was stirred for 5 min until a homogeneous mixture was obtained. The mixture was then filtered through a filter paper (Whatman-1) and washed the residue 10 times with minimum volume of distilled methanol to collect the ILs that might present in the residue. After complete removal, all the filtrates were combined together and the purity was checked by means of TLC. Finally, the ILs were isolated from this filtrate by rotary evaporation and were dried in vacuum at 70°C for three days. After purification, all the ILs became colorless. The purified ILs were then fully characterized by using ^{1}H NMR spectroscopy ([D_6]DMSO and D_2O). For comparison, the ^{1}HNMR spectra of sodium ascorbate and one of theses ILs, [C_2mim][A] were recorded by using D_2O as a solvent.

Ascorbic acid: ^{1}H NMR (300 MHz, [D_6]DMSO, TMS): $\delta = 4.62$–4.61 (d, five member ring H), 3.90–3.81 (m, $J = 6.5$ Hz, -CH), 3.69–3.65 (m, $J = 6.0$, -CH_2).

Sodium ascorbate: ^{1}H NMR (300 MHz, D_2O, TMS): $\delta = 4.38$–4.37 (d, five member ring H), 3.91–3.87 (q, $J = 6.0$ Hz, -CH), 3.67–3.62 ppm (d, -CH_2).

1-Ethyl-3-methylimidazolium ascorbate: ^{1}H NMR (300 MHz, DMSO [D_6], TMS): $\delta = 9.1$ (s, Immidazole ring H), 7.75 (s, Immidazole ring H), 7.67 (s, Immidazole ring H), 4.21–4.13 (q, $J = 7.4$ Mz, -NCH_2), 3.8 (s, -NCH_3), 1.42–1.37 ppm (t, $J = 7.3$ Mz, -CH_3); ^{1}H NMR (300 MHz; D_2O; TMS): $\delta = 8.58$ (s. Immidazole ring H), 7.35 (s, Immidazole ring H), 7.29 (s, Immidazole ring H), 4.40–4.38 (d, 1H), 4.13–4.06 (q, $J = 6.0$ Hz, 2H), 3.39–3.98 (d, 1H), 3.70 (s, 3H), 3.68–3.62 (m, $J = 6.0$ Hz, 2H), 1.39–1.34 ppm (t, $J = 7.4$ Mz, 3H); MS (EI, 35 eV): m/z: 111 (M^+ 100%); elemental analysis calcd (%) for $C_{12}H_{18}N_2O_6$ (286): C 50.34, H 6.29, N 9.79; found: C 50.12, H 6.64, N 9.30.

1-Butyl-3-methylimidazolium ascorbate: ^{1}H NMR (300 MHz, [D_6]DMSO, TMS): $\delta = 9.05$ (s, Immidazole ring H), 7.71 (s, Immidazole ring H), 7.65 (s, Immidazole ring H), 4.15–4.10 (t, $J = 6.9$ Hz, -NCH_2), 3.81 (s, -NCH_3), 1.76–1.71 (m, CH_2), 1.27–1.19 (m, CH_2), 0.90–0.85 ppm (t, $J = 7.1$ Hz, CH_3); MS (EI, 35 ev): m/z: 139 (M^+ 100%); elemental analysis calcd (%) for $C_{14}H_{22}N_2O_6$ (314): C 53.50, H 7.00, N 8.917; found: C 53.21, H 7.29, N 8.54.

1-Hexyl-3-methylimidazolium ascorbate: ^{1}H NMR (300 MHz, [D_6]DMSO, TMS): $\delta = 9.05$ (s, Immidazole ring H), 7.73 (s, Immidazole ring H), 7.65 (s, Immidazole ring H), 4.12 (bs, -NCH_2), 3.82 (s, -NCH_3), 1.75 (bs, -CH_2), 1.24 (bs, 3 -CH_2), 0.84 ppm (bs, -CH_3); MS (EI, 35 eV): m/z: 167 (M^+ 100%); elemental analysis calcd (%) for $C_{16}H_{26}N_2O_6$ (342): C 56.14, H 7.6, N 8.1; found: C 56.35, H 7.73, N 7.84.

1-Octyl-3-methylimidazolium ascorbate: ^{1}H NMR (300 MHz, [D_6]DMSO, TMS): $\delta = 9.04$ (s, Immidazole ring H), 7.72 (s, Immidazole ring H), 7.65 (s, Immidazole ring H), 4.14–4.09 (t, $J = 7.1$ Hz, -NCH_2), 3.81 (s, -NCH_3), 1.77–1.72 (m, -CH_2), 1.22 (bs, 5-CH_2), 0.85–0.80 ppm (t, $J = 7.0$ Hz, -CH_3); MS (EI, 35 eV): m/z: 195 (M^+ 100%); elemental analysis calcd (%) for $C_{18}H_{30}N_2O_6$ (370): C 58.37, H 8.1, N 7.56; found: C 58.22, H 8.21, N 7.40.

1-Decyl-3-methylimidazolium ascorbate: ^{1}H NMR (300 MHz, [D_6]DMSO, TMS): $\delta = 9.04$ (s, Immidazole ring H), 7.72 (s, Immidazole ring H), 7.65 (s, Immidazole ring H), 4.13–4.09 (t, $J = 7.1$ Hz, -NCH_2), 3.94 (s, -NCH_3), 1.76–1.74 (m, -CH_2), 1.21 (bs, 7-CH_2), 0.85–0.80 ppm (t, $J = 6.3$ Hz, -CH_3); MS (EI, 35 eV): m/z: 223 (M^+ 100%); elemental analysis calcd (%) for $C_{14}H_{22}N_2O_6$ (398): C 60.30, H 8.54, N 7.03; found: C 60.55, H 8.78, N 6.75.

Synthesis of gold nanostructures using different ILs: In a typical synthesis, an aliquot (0.1 mL, 10 mM) of each of IL solution was added separately

to an aqueous $HAuCl_4$ solution (1.9 mL of 0.526 mM) taken in labeled glass vials to get a mole ratio of IL to $HAuCl_4$ ($R = 1.0$; IL is acting as reducing agent for $HAuCl_4$) under constant magnetic stirring. Two more sets of reactions were also carried out at varying R values. That is, the concentration of IL was varied, keeping the concentration of $HAuCl_4$ the same (see table 2) under reaction conditions similar to that maintained in the previous reaction. The progress of the formation of gold nanostructures was then followed through visualization of the color change of the colloidal suspension as well as by using UV/Vis spectroscopy.

Acknowledgements

S. Si thanks CSIR, India for the fellowship. This research was supported by the grants from both DBT and CSIR, India. Thanks are also owed to the partial support from the Nanoscience and Nanotechnology Initiatives, DST, India.

[1] S. A. Maier, M. L. Brongersma, P. G. Kik, S. Meltzer, A. A. G. Requicha, H. A. Atwater, *Adv. Mater.* **2001**, *13*, 1501.
[2] R. Narayanan, M. A. El-Sayed, *J. Phys. Chem. B* **2005**, *109*, 12663.
[3] M. H. Rashid, R. R. Bhattacharjee, A. Kotal, T. K. Mandal, *Langmuir* **2006**, *22*, 7141.
[4] R. F. Aroca, R. A. Alvarez-Puebla, N. Pieczonka, S. Sanchez-Cortez, J. V. Garcia-Ramos, *Adv. Colloid Interface Sci.* **2005**, *116*, 45.
[5] J. M. Polak, I. M. Varndell, *Immunolabeling for electron microscopy*, Elsevier Pub, Amsterdam, **1984**.
[6] R. Elghanian, J. J. Storhoff, R. C. Mucic, R. L. Letsinger, C. A. Mirkin, *Science* **1997**, *277*, 1078.
[7] P. Sharma, S. Brown, G. Walter, S. Santra, B. Moudgil, *Adv. Colloid Interface Sci.* **2006**, *123–126*, 471.
[8] A. Gole, C. J. Murphy, *Chem. Mater.* **2004**, *16*, 3633.
[9] H. M. Chen, C. F. Hsin, R. S. Liu, J.-F. Lee, L.-Y. Jang, *J. Phys. Chem. C* **2007**, *111*, 5909.
[10] H. C. Chu, C. H. Kuo, M. H. Huang, *Inorg. Chem.* **2006**, *45*, 808.
[11] M. H. Rashid, T. K. Mandal, *J. Phys. Chem. C* **2007**, *111*, 16750.
[12] M. H. Rashid, R. R. Bhattacharjee, T. K. Mandal, *J. Phys. Chem. C* **2007**, *111*, 9684.
[13] C. Li, K. L. Shuford, Q. H. Park, W. Cai, Y. Li, E. J. Lee, S. O. Cho, *Angew. Chem.* **2007**, *119*, 3328; *Angew. Chem. Int. Ed.* **2007**, *46*, 3264.
[14] D. Seo, J. C. Park, H. Song, *J. Am. Chem. Soc.* **2006**, *128*, 14863.
[15] R. Jin, Y. Cao, C. A. Mirkin, K. L. Kelly, G. C. Schazt, J. G. Zheng, *Science* **2001**, *294*, 1901.
[16] K. Kwon, K. Y. Lee, Y. W. Lee, M. Kim, J. Heo, S. J. Ahn, S. W. Han, *J. Phys. Chem. C* **2007**, *111*, 1161.
[17] S. Randstrom, G. B. Appetecchi, C. Lagergren, A. Morenoa, S. Passerini, *Electrochim. Acta* **2007**, *53*, 1837.
[18] T. Welton, *Chem. Rev.* **1999**, *99*, 2071.
[19] J. H. Davis Jr. , P. A. Fox, *Chem. Commun.* **2003**, 1209.
[20] A. E. Visser, R. P. Swatloski, W. M. Reichert, R. Mayton, S. Sheff, A. Wierzbicki, J. H. Davis, Jr., T. Robin, D. Rogers, *Chem. Commun.* **2001**, *1*, 135.
[21] M. J. Earle, K. R. Seddon, *Pure Appl. Chem.* **2000**, *72*, 1391.
[22] P. Bonhote, A. P. Dias, N. Papageorgiou, K. Kalyanasundaram, M. Gratzel, *Inorg. Chem.* **1996**, *35*, 1168.
[23] J. Kagimoto, K. Fukumoto, H. Ohno, *Chem. Commun.* **2006**, 2254.
[24] K. Fukumoto, M. Yoshizawa, H. Ohno, *J. Am. Chem. Soc.* **2005**, *127*, 2398.
[25] S. T. Handy, M. Okello, G. Dickenson, *Org. Lett.* **2003**, *5*, 2513.
[26] E. B. Carter, S. L. Culver, P. A. Fox, R. D. Goode, I. Ntai, M. D. Tickell, R. K. Traylor, N. W. Hoffman, J. H. Davis Jr. , *Chem. Commun.* **2004**, 630.
[27] J. Pernak, I. Goc, I. Mirska, *Green Chem.* **2004**, *6*, 323.
[28] M. J. Earle, P. B. McCormac, K. R. Seddon, *Green Chem.* **1999**, *1*, 23.
[29] J. Dupont, G. S. Fonseca, A. P. Umpierre, P. F. P. Fichtner, S. R. Teixeira, *J. Am. Chem. Soc.* **2002**, *124*, 4228.
[30] C. W. Scheeren, G. Machado, J. Dupont, P. F. P. Fichtner, S. R. Texeira, *Inorg. Chem.* **2003**, *42*, 4738.
[31] K. S. Kim, D. Demberelnyamba, H. Lee, *Langmuir* **2004**, *20*, 556.
[32] M. Antonietti, D. Kuang, B. Smarsly, Y. Zhou, *Angew. Chem.* **2004**, *116*, 5096; *Angew. Chem. Int. Ed.* **2004**, *43*, 4988.
[33] K. S. Kim, S. Choi, J. H. Cha, S. H. Yeon, H. Lee, *J. Mater. Chem.* **2006**, *16*, 1315.
[34] G.-T. Wei, Z. Yang, C.-Y. Lee, H.-Y. Yang, C. R. C. Wang, *J. Am. Chem. Soc.* **2004**, *126*, 5036.
[35] R. Tatumi, H. Fujihara, *Chem. Commun.* **2005**, 83.
[36] H. Itoh, K. Naka, Y. Chujo, *J. Am. Chem. Soc.* **2004**, *126*, 3026.
[37] S. Chen, Y. Liu, G. Wu, *Nanotechnology* **2005**, *16*, 2360.
[38] S. Guo, F. Shi, Y. Gu, J. Yang, Y. Deng, *Chem. Lett.* **2005**, *34*, 830.
[39] Y. Jin, P. Wang, D. Yin, J. Liu, L. Qin, N. Yu, G. Xie, B. Li, *Colloids Surf. A* **2007**, *302*, 366.
[40] J. Zhu, Y. Shen, A. Xie, L. Qiu, Q. Zhang, S. Zhang, *J. Phys. Chem. C* **2007**, *111*, 7629.
[41] M. A. Firestone, M. L. Dietz, S. Seifert, S. Trasobares, D. J. Miller, N. J. Zaluzec, *Small* **2005**, *1*, 754.
[42] F. Endres, S. Zein El Abedin, *Phys. Chem. Chem. Phys.* **2006**, *8*, 2101.
[43] G. S. Fonseca, A. P. Umpierre, P. F. P. Fichtner, S. R. Teixeira, J. Dupont, *Chem. Eur. J.* **2003**, *9*, 3263.
[44] A. I. Bhatt, A. Mechler, L. L. Martin, A. M. Bond, *J. Mater. Chem.* **2007**, *17*, 2241.
[45] J. Huang, T. Jiang, B. Han, H. Gao, Y. Chang, G. Zhao, W. Wu, *Chem. Commun.* **2003**, 1654.
[46] Y. J. Zhu, W. W. Wang, R. J. Qi, X. L. Hu, *Angew. Chem.* **2004**, *116*, 1434; *Angew. Chem. Int. Ed.* **2004**, *43*, 1410.
[47] Y. Wang, H. Yang, *J. Am. Chem. Soc.* **2005**, *127*, 5316.
[48] S. Z. El Abedin, M. Polleth, S. A. Meiss, J. Janek, F. Endres, *Green Chem.* **2007**, *9*, 549.
[49] S. A. Meiss, M. Rohnke, L. Kienle, S. Z. El Abedin, F. Endres, J. Janek, *ChemPhysChem* **2007**, *8*, 50.
[50] S. Si, R. R. Bhattacharjee, A. Banerjee, T. K. Mandal, *Chem. Eur. J.* **2006**, *12*, 1256.
[51] S. Si, E. Dinda, T. K. Mandal, *Chem. Eur. J.* **2007**, *13*, 9850.
[52] S. Si, T. K. Mandal, *Chem. Eur. J.* **2007**, *13*, 3160.
[53] R. R. Bhattacharjee, A. K. Das, D. Halder, S. Si, A. Banerjee, T. K. Mandal, *J. Nanosci. Nanotechnol.* **2005**, *5*, 1141.
[54] J. Wagner, J. M. Kohler, *Nano Lett.* **2005**, *5*, 685.
[55] P. K. Vemula, U. Aslam, V. A. Mallia, G. John, *Chem. Mater.* **2007**, *19*, 138.
[56] D. V. Goia, E. Matijevic, *New J. Chem.* **1998**, *22*, 1203.
[57] C. J. Murphy, T. K. Sau, A. M. Gole, J. Orendorff, J. Gao, L. Gou, S. E. Hunyadi, T. Li, *J. Phys. Chem. B* **2005**, *109*, 13857.
[58] L. Gou, C. J. Murphy, *Chem. Mater.* **2005**, *17*, 3668.
[59] N. Borisenko, S. Z. El Abedin, F. Endres, *J. Phys. Chem. B* **2006**, *110*, 6250.
[60] K. Binnemans, *Chem. Rev.* **2005**, *105*, 4148.
[61] A. E. Bradley, C. Hardacre, J. D. Holbrey, S. Johnston, S. E. J. McMath, M. Nieuwenhuyzen, *Chem. Mater.* **2002**, *14*, 629.
[62] C. H. Kuo, M. H. Huang, *Langmuir* **2005**, *21*, 2012.

Received: January 2, 2008
Published online: May 9, 2008

